International Workshop on Stellar Spectral Libraries
ASI Conference Series, 2012, Vol. 6, pp 23 – 30
Edited by Ph. Prugniel & H. P. Singh

An atlas of L-T transition brown dwarfs with VLT/XShooter

F. Marocco[1]*, A. C. Day-Jones[2], H. R. A. Jones[1] and D. J. Pinfield[1]
[1]*Centre for Astrophysics Research, STRI, University of Hertfordshire, Hatfield AL10 9AB, UK*
[2]*Universidad de Chile, Santiago, Casilla 36-D, Chile*

Abstract. In this contribution we present the first results from a large observing campaign we are carrying out using VLT/Xshooter to obtain spectra of a large sample (~250 objects) of L-T transition brown dwarfs. Here we report the results based on the first ~120 spectra already obtained. The large sample, and the wide spectral coverage (300-2480 nm) given by Xshooter, will allow us to do a new powerful analysis, at an unprecedent level. By fitting the absorption lines of a given element (e.g. Na) at different wavelengths we can test ultracool atmospheric models and draw for the first time a 3D picture of stellar atmospheres at temperatures down to 1000K. Determining the atmospheric parameters (e.g. temperature, surface gravity and metallicity) of a big sample of brown dwarfs, will allow us to understand the role of these parameters on the formation of their spectra. The large number of objects in our sample also will allow us to do a statistical significant test of the birth rate and initial mass function predictions for brown dwarfs. Determining the shape of the initial mass function for very low mass objects is a fundamental task to improve galaxy models, as recent studies (van Dokkum & Conroy 2010) have shown that low-mass objects dominate in massive elliptical galaxies.

Keywords : stars: low mass, brown dwarfs - binaries: spectroscopic

1. Introduction

Our current description of the atmospheres of extremely-cool low-mass objects (T< 2500 K, M< 0.08 $M_{\odot}$, known as brown dwarfs, Kumar 1963) presents a number of unresolved problems. The most outstanding one is the modelling of the dust settling

*email: f.marocco@herts.ac.uk

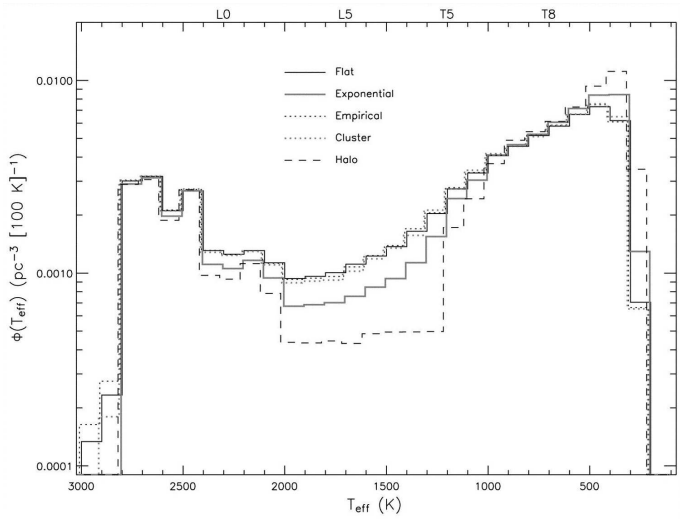

Figure 1. The results of Monte Carlo simulations from Burgasser (2004), assuming a mass function in the form $\Psi(M) \propto M^{-0.5}$ and different birth rates.

process taking place at the transition between spectral types L and T. Current proposed models are unable to explain the rapidity of the process (Tsuji & Nakajima 2003; Knapp et al. 2004; Burrows, Sudarsky & Hubeny 2006). To better constrain present models, we are carrying out an observing campaign using the VLT and the Xshooter spectrograph, to take good signal-to-noise spectra (S/N∼30) of a large sample (∼250 objects) spanning the L to T spectral classes. The main goal of this program is to put a statistically significant constraint on the low mass birth rate. Simulations have shown that the L-T transition range is an ideal probe of the birth rate. In particular we can see from Figure 1 (from Burgasser 2004) that different assumptions on the brown dwarf birth rate give similar results especially in the late M - early L spectral regime, as well as in the late-T range, while more dramatic differences appear to be seen at the L-T transition. Moreover, a Salpeter-like initial mass function would predict an increasing number of objects as the mass decreases. Results obtained so far by the large sky surveys (e.g. SDSS, 2MASS and UKIDSS) indicate that at the extremely cool end the initial mass function differs from that of normal stars, suggesting it likely decreases with mass. However, the lack of a significant sample for which atmospheric parameters have been robustly determined, has so far prevented us to find a definitive solution to the problem.

2. Candidates selection

Candidates were selected from the United Kingdom Infrared Telescope Deep Sky Survey (hereafter UKIDSS) Large Area Survey (hereafter LAS) 7^{th} data release. We selected objects with a measured MKO system J magnitude brighter than 18.1 (the

12σ detection limit of the LAS). We eliminated objects with uncertainties on the measured YJH magnitudes greater than 30%. To segregate L and T dwarfs we applied a colour cut of Y-J>0.8, as this selection has been proved to be substantially free of M dwarfs (Hewett et al. 2006). This list was then cross-matched with SDSS DR7, and applied a colour cut of z-J>2.4 in order to eliminate contaminant QSOs and high redshift galaxies (Chiu et al. 2006; Scholz 2010). SDSS and UKIDSS images of each target were visually inspected to remove remaining contaminants (e.g. high-redshift galaxies). Finally we removed all previously known objects. This selection yielded a final sample of 263 objects from 2000 deg^2 of LAS sky. Given that the expected number for such an area of the sky is of 250 objects, this suggests that our sample is essentially free of contamination.

3. Observations and analysis

The project has so far been awarded 20 nights, during ESO observing periods 86 to 88. We observed 117 objects from our sample during the first 16 night of the project. Targets are observed in nodding mode with a dithering offset of 5 arcseconds. To allow for telluric correction we observe a telluric standard star immediately before or after each target, at a similar airmass and close in the sky. The data were reduced using the Xshooter pipeline version 1.3.7. The pipeline performs all the basic reduction steps, such as bias and dark subtraction, flat fielding and pair-wise subtraction to remove the OH airglow lines. The different echelle orders on each of Xshooter's three arms (UVB, VIS and NIR) are then rectified and merged. Finally we extract the spectra using standard IRAF routines, and the different arms are merged using our own IDL code. Telluric lines are removed by dividing the target's spectra by the associated telluric (after hydrogen absorption lines have been removed) and multiplying by the appropriate atmospheric model, taken from the Kurucz atlas. Photometric calibration is performed using the telluric stars measured JHK magnitudes (in 2MASS photometric system).

The properties of the objects observed are summarized in Table 1 (from Day-Jones et al. 2013). For each object we list name, signal-to-noise ratio in both the VIS and the NIR arm and the derived spectral type. We confirm 108 of our targets as new L or T dwarfs, 7 turned out to be late M dwarfs, while only 2 are early type objects. Given that late M dwarfs are still interesting objects for our project, the total number of contaminants is 2 out of 117 objects observed, giving a level of contamination of 1.7%. This number confirms, although only preliminarily, the effectiveness of the selection criteria applied. The spectral types of our objects were determined via chi-squared fitting with standard templates taken from the SpeX-Prism online library[1]. In Figure 2 we show two examples of this fitting procedure.

We also investigated the possibility of unresolved binaries within our sample, us-

[1] http://pono.ucsd.edu/~adam/browndwarfs/spexprism

Table 1. The list of objects observed. For each target we present name, S/N in the VIS and NIR arm and the spectral type derived.

Target name	VIS S/N	NIR S/N	Spectral type	Target name	VIS S/N	NIR S/N	Spectral type
BRLT1	4.54	29.7	L9.0 ± 0.5	BRLT56	3.01	22.8	L1.5 ± 1.0
BRLT2	4.72	18.8	L1.0 ± 1.0	BRLT57	3.93	26.6	L0.0 ± 1.0
BRLT3	5.21	32.8	L9.0 ± 1.0	BRLT58	5.09	27.1	L5.5 ± 1.0
BRLT6	5.32	25.2	L3.0 ± 1.0	BRLT60	4.11	27.9	L1.0 ± 1.0
BRLT7	7.61	20.9	M8.0 ± 1.0	BRLT62	2.64	26.8	L5.0 ± 1.0
BRLT8	5.18	31.0	L8.5 ± 0.5	BRLT64	5.26	29.5	L4.0 ± 0.5
BRLT9	8.01	30.7	L1.0 ± 1.0	BRLT66	4.82	27.5	L5.0 ± 0.5
BRLT10	2.39	26.5	L9.0 ± 0.5	BRLT69	5.26	18.0	L1.0 ± 0.5
BRLT12	4.30	18.7	L3.0 ± 1.0	BRLT71	3.19	25.1	L1.5 ± 0.5
BRLT14	7.56	29.8	L0.0 ± 0.5	BRLT72	5.73	30.5	M9.0 ± 0.5
BRLT15	2.40	21.6	T2.0 ± 2.0	BRLT73	2.81	21.3	L1.0 ± 0.5
BRLT16	3.66	22.8	L3.5 ± 0.5	BRLT74	1.61	18.3	L9.5 ± 1.0
BRLT18	5.79	29.0	L0.0 ± 1.0	BRLT75	4.69	18.6	M9.0 ± 1.0
BRLT20	5.12	20.7	L1.0 ± 1.0	BRLT76	4.75	27.7	L5.5 ± 0.5
BRLT21	3.73	29.5	L3.5 ± 0.5	BRLT82	5.57	27.4	L1.0 ± 0.5
BRLT22	5.84	17.7	M9.5 ± 0.5	BRLT83	5.08	17.2	M8.0 ± 1.0
BRLT24	4.17	23.9	L3.5 ± 0.5	BRLT84	4.07	23.7	L3.5 ± 0.5
BRLT26	4.14	24.2	L5.5 ± 0.5	BRLT88	3.37	26.2	L4.0 ± 1.0
BRLT27	2.22	27.6	T1.0 ± 0.5	BRLT90	9.17	13.4	M2.5 ± 1.0
BRLT30	6.39	53.3	L5.0 ± 0.5	BRLT91	1.27	19.2	T3.0 ± 0.5
BRLT31	6.18	27.6	L4.0 ± 1.0	BRLT92	5.60	31.7	L1.0 ± 0.5
BRLT32	5.76	25.0	L1.5 ± 0.5	BRLT97	4.01	23.3	L0.0 ± 1.0
BRLT33	2.93	20.9	L3.5 ± 0.5	BRLT103	3.80	25.4	L5.5 ± 0.5
BRLT35	5.86	21.6	M9.5 ± 0.5	BRLT105	3.95	35.6	L5.0 ± 0.5
BRLT37	4.84	26.0	L5.0 ± 0.5	BRLT122	3.08	18.8	L1.0 ± 0.5
BRLT38	4.14	31.9	T1.0 ± 0.5	BRLT129	5.01	31.4	L5.0 ± 1.0
BRLT39	7.77	29.8	L5.0 ± 1.0	BRLT131	1.79	40.2	T3.0 ± 0.5
BRLT42	5.75	23.6	M9.0 ± 0.5	BRLT135	6.86	39.9	T2.5 ± 0.5
BRLT44	4.30	28.6	L5.0 ± 1.0	BRLT137	2.87	21.5	L4.5 ± 0.5
BRLT45	3.76	16.7	T1.0 ± 0.5	BRLT138	3.09	35.1	L2.0 ± 1.0
BRLT46	3.84	21.6	L0.5 ± 0.5	BRLT142	4.24	31.0	L2.5 ± 0.5
BRLT48	2.93	27.6	L4.5 ± 0.5	BRLT147	1.31	29.2	T3.0 ± 0.5
BRLT50	∼1	7.26	T7.0 ± 0.5	BRLT155	2.44	34.2	L3.0 ± 1.0
BRLT51	4.59	22.9	L3.0 ± 1.0	BRLT162	8.46	66.5	L0.5 ± 0.5
BRLT52	6.55	29.1	L5.5 ± 0.5	BRLT171	3.81	60.1	L5.0 ± 0.5

Table 1. Continued.

Target name	VIS S/N	NIR S/N	Spectral type	Target name	VIS S/N	NIR S/N	Spectral type
BRLT176	1.71	27.5	L4.0 ± 1.0	BRLT311	2.93	16.2	T3.0 ± 0.5
BRLT179	∼1	7.79	T4.5 ± 0.5	BRLT312	4.38	22.9	T0.0 ± 0.5
BRLT181	2.62	22.4	L1.0 ± 1.0	BRLT313	6.34	42.0	L3.5 ± 0.5
BRLT186	8.58	64.7	L1.0 ± 1.0	BRLT314	1.71	28.2	L7.5 ± 0.5
BRLT190	∼1	13.0	T4.0 ± 0.5	BRLT315	4.96	25.3	L1.0 ± 1.0
BRLT197	1.73	34.1	T2.0 ± 1.0	BRLT316	4.41	20.3	L1.0 ± 0.5
BRLT202	2.01	21.5	T2.5 ± 0.5	BRLT317	13.7	77.1	L1.0 ± 1.0
BRLT203	2.63	38.4	T3.0 ± 1.0	BRLT318	4.91	21.7	L1.0 ± 0.5
BRLT207	2.40	49.9	L7.0 ± 0.5	BRLT320	4.49	19.7	L1.0 ± 0.5
BRLT210	1.46	32.2	L4.5 ± 0.5	BRLT321	1.26	16.0	T4.0 ± 0.5
BRLT212	8.10	84.9	L8.0 ± 2.0	BRLT322	5.48	27.7	L5.0 ± 0.5
BRLT219	∼1	14.7	T3.0 ± 0.5	BRLT323	3.83	37.8	T0.0 ± 1.0
BRLT232	1.94	39.3	T2.5 ± 0.5	BRLT325	2.39	18.0	T2.0 ± 1.0
BRLT234	5.67	41.8	L7.0 ± 1.0	BRLT328	4.23	23.4	L0.5 ± 1.0
BRLT236	3.11	20.3	L3.5 ± 0.5	BRLT330	5.20	20.6	L1.0 ± 1.0
BRLT258	4.02	43.3	L5.0 ± 1.0	BRLT331	5.45	21.9	L1.0 ± 2.0
BRLT275	2.81	22.7	T2.0 ± 2.0	BRLT332	7.87	27.7	L2.0 ± 2.0
BRLT287	2.83	52.0	T3.0 ± 0.5	BRLT333	1.70	21.5	T2.0 ± 0.5
BRLT295	4.86	48.7	L6.5 ± 2.0	BRLT334	4.06	33.9	L3.5 ± 0.5
BRLT299	3.68	48.7	L4.0 ± 1.0	BRLT335	3.75	24.5	L4.0 ± 1.0
BRLT305	1.94	19.3	L5.5 ± 1.0	BRLT338	3.44	18.2	L1.0 ± 1.0
BRLT306	1.71	25.7	L4.5 ± 1.0	BRLT343	3.67	28.0	L9.0 ± 1.0
BRLT307	7.84	27.2	L1.0 ± 0.5	BRLT344	4.17	26.8	T0.0 ± 1.0

ing the spectral indices and criteria defined in Burgasser et al. (2010). The selection essentially makes use of a series of spectral indices to segregate possible unresolved binaries. The spectral indices used take into account the flux ratio of the prominent molecular absorption bands of water and methane over the flux emitted in the J, H and K band. In Fig. 3 we show the selection criteria applied to the different index-index and index-spectral type plots. Objects that match at least two criteria are called "weak candidates", while objects matching at least three criteria are called "strong candidates". With this method we identified 12 strong candidates and 10 weak candidates. These binary candidates are now being analysed to confirm or disprove their binary nature and also to try and deconvolve the spectra of the two components, using our own library of synthetic unresolved binary templates.

4. Future work and conclusions

The wide wavelength coverage delivered by Xshooter allows us to do a unprecedented analysis of the spectra of our objects. By looking at the absorption features of a given

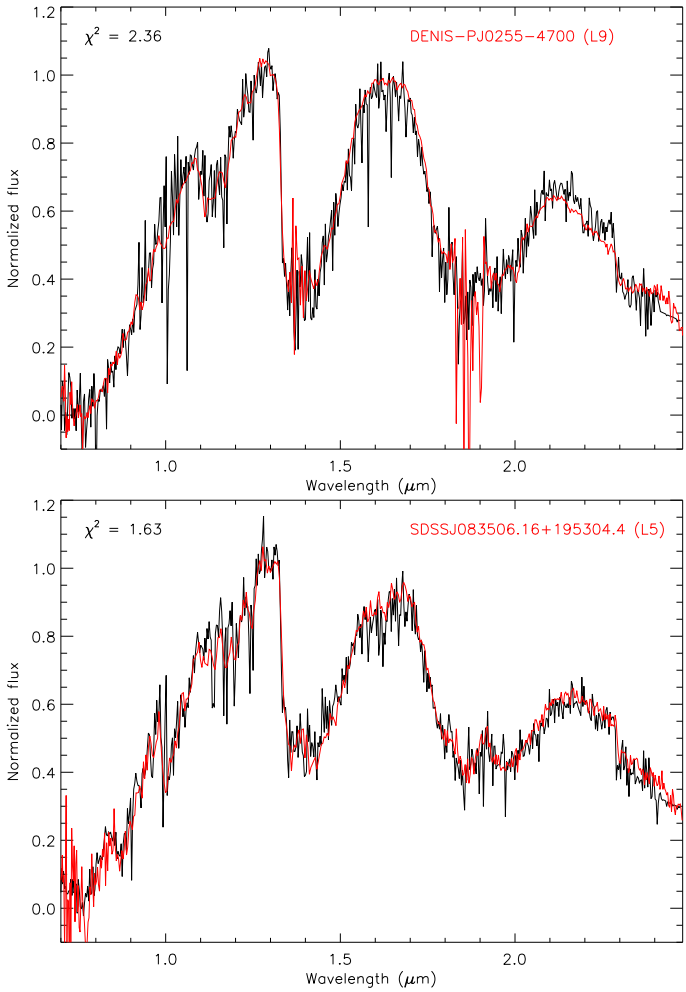

Figure 2. Two brown dwarfs from our sample. Overplotted in red we show the best fit standard template. On the top panel we present the L9 BRLT10, in the bottom panel the L5 BRLT105.

element (e.g. Na) at different wavelengths, we can test the atmospheric models at different optical depth, providing strong insights. Comparing the spectra observed with the spectral standards and the benchmark objects known to date, we can also identify spectroscopically peculiar objects (e.g. subdwarfs). These objects can offer a more detailed view of the effects of changes in gravity and metallicity on the dust settling process, therefore on the formation of the spectra of L-T transition brown dwarfs.

Once the observations are complete, we will also be able to put strong constraints on the birth rate of brown dwarfs, comparing our observational results with the results

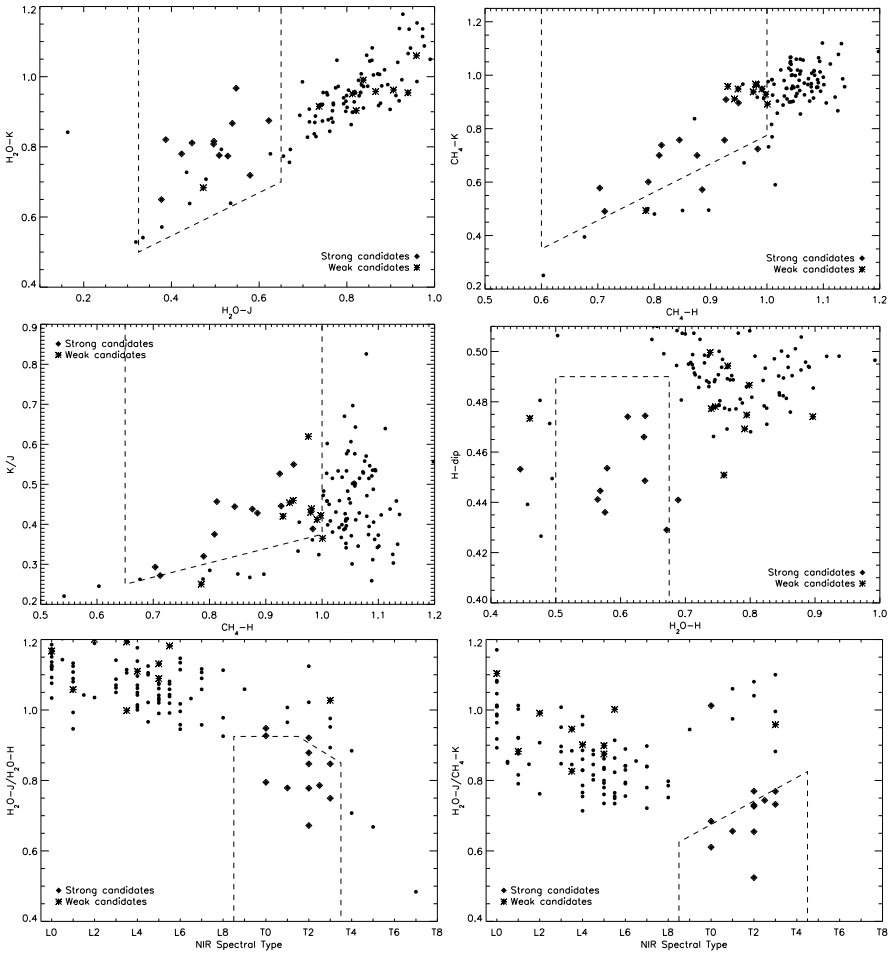

Figure 3. The selection criteria applied for binary candidate segregation. In each plot the dashed line delimits the area of unresolved binaries. Strong candidates are marked with diamonds, weak candidates with asterisks.

of numeric simulations like those shown in Fig. 1 (Burgasser 2004), and investigate the implications for the initial mass function and the binary fraction of brown dwarfs in the L-T transition.

Acknowledgements

ADJ is supported by a Fondecyt Postdoctorado under project number 3100098. ADJ is also partially supported by the Joint Committee ESO-Government of Chile. This research has made use of: the SIMBAD database operated at CDS France; the SpeX

Prism Spectral Libraries, maintained by Adam Burgasser at http://pono.ucsd.edu/~adam/browndwarfs/spexprism; and, the M, L, and T dwarf compendium housed at dwarfArchives.org and maintained by Chris Gelino, Davy Kirkpatrick, and Adam Burgasser.

References

Burgasser A. J., 2004, ApJS, 155, 191
Burgasser A. J., Cruz K. L., Cushing M., Gelino C. R., Looper D. L., Faherty J. K., Kirkpatrick J. D., Reid I. N., 2010, ApJ, 710, 1142
Burrows A., Sudarsky D., Hubeny I., 2006, ApJ, 640, 1063
Chiu K., Fan X., Leggett S. K., Golimowski D. A., Zheng W., Geballe T. R., Schneider D. P., Brinkmann J., 2006, AJ, 131, 2722
Hewett P. C., Warren S. J., Leggett S. K., Hodgkin S. T., 2006, MNRAS, 367, 454
Day-Jones, A. C., 2013, MNRAS, 430, 1171
Knapp G. R., et al., 2004, AJ, 127, 3553
Kumar S. S., 1963, ApJ, 137, 1121
Scholz R.-D., 2010, A&A, 515, A92
Tsuji T., Nakajima T., 2003, ApJ, 585, L151
van Dokkum P. G., Conroy C., 2010, Nature, 468, 940